Int. J. Electrochem. Sci., 8 **(2013)** 753 - 772

International Journal of
ELECTROCHEMICAL
SCIENCE
www.electrochemsci.org

Novel Iron-Cobalt Derivatised Lithium Iron Phosphate Nanocomposite for Lithium Ion Battery Cathode

Chinwe O. Ikpo[1], *Charl J. Jafta*[2], *Kenneth I. Ozoemena*[2], *Natasha West*[1], *Njagi Njomo*[1], *Nazeem Jahed*[1], *Priscilla G. Baker*[1] *and Emmanuel I. Iwuoha*[1,*]

[1] SensorLab, Department of Chemistry, University of Western Cape, Moderddam Road, Bellville, Cape Town 7535, South Africa
[2] Energy and Processes Division, Materials Science and Manufacturing, Council for Scientific and Industrial Research (CSIR) Pretoria 0001, South Africa
[*]E-mail: eiwuoha@uwc.ac.za

Received: 5 November 2012 / *Accepted:* 11 December 2012 / *Published:* 1 January 2013

Described herein is the electrochemical study conducted on lithium ion battery cathode material consisting of composite of lithium iron phosphate ($LiFePO_4$), iron-cobalt derivatised carbon nanotubes (FeCo-CNT) and polyaniline (PA) nanomaterials (LiFePO4/FeCoCNT-PA); and pristine $LiFePO_4$. The design of the nanocomposite electrode involves first, the attachment of FeCo nanoparticles unto the nanotubes matrix via in situ reductive precipitation of the metal precursors within a CNT suspension. Results from High Resolution Transmission Electron Microscopy show the successful attachment of FeCo nanoparticles to the CNTs. The composite cathode exhibits better reversibility and kinetics than the pristine $LiFePO_4$ due to the presence of the conductive additives in the former. This is demonstrated in the values of the diffusion coefficient (D) and standard rate constant (k_s) determined through cyclic voltammetry. For the composite cathode D = 1.0 x 10^{-9} cm^2 s^{-1} and k_s = 7.05 x 10^{-7} cm s^{-1} whereas the pristine electrode has values of 4.81 x 10^{-11} cm^2 s^{-1} and 2.68 x 10^{-7} cm s^{-1} for D and k_s, respectively. Similar trend is observed in the results obtained from electrochemical impedance spectroscopy.

Keywords: Lithium iron phosphate composite cathode, charge-discharge reversibility, Klingler and Kochi equation, standard rate constant, lithium ion diffusion

1. INTRODUCTION

The global quest for clean energy and a green planet has made the development of sustainable and efficient energy storage systems inevitable. As an electrochemical energy storage device, a battery is of strategic importance. Batteries are needed to store electricity from renewable sources, power green technologies such as electric vehicles, as well as myriads of portable electronic devices that are

constantly released to the consumer world [1-2]. The lithium-ion batteries are top among emerging technologies designed to meet the increasing market demands which are in tandem with technological advancements. However, the development, performance and cost of lithium-ion batteries are mainly limited by the properties of the cathode materials [3-5]. The predominant cathode material is $LiCoO_2$. This material has the disadvantages of being unsafe, toxic, and costly. A search for alternative materials with better characteristics became imperative and led to the discovery of olivine $LiFePO_4$, whose electrochemical activity was first reported by Pahdi *et al* [6]. Delithiation of $LiFePO_4$ during charging gives $FePO_4$ in which the Fe^{2+} ions are oxidized to Fe^{3+}, leaving the 3D olivine framework intact. Its major drawback is that of having low electronic conductivity [7-8] and lithium-ion diffusivity [6-7, 9] which affects its rate capabilities and applications. Considerable efforts have been made to overcome these limitations [10-16]. Whittingham *et al*. [17] indicated that multi-walled carbon nanotubes (MWCNTs) in pure $LiFePO_4$ enhanced the electronic conductivity of the final product. Huang and Goodenough [18] showed that significantly improved capacity and rate capability can be achieved in $LiFePO_4$/polymer composite cathodes.

In this work $LiFePO_4$/carbon nanotubes/polyaniline composite cathode (with the carbon nanotubes previously functionalised with iron-cobalt nanoparticles) was synthesized and to the best of our knowledge this has not been reported. Iron-cobalt nanoparticles due to their porous structure provide viable routes for the facile transfer of electrons during lithium ion deinsertion/insertion in a 3-D nanonetwork that is formed between the carbon nanotubes and adjacent $LiFePO_4$ particles. It is expected that the iron-cobalt derivatised carbon nanotubes, in combination with polyaniline conducting polymer, will bring about synergistic effects in the electrochemical properties and performance of lithium iron phosphate cathode in a lithium ion cell.

Furthermore, the investigation and understanding of the parameters which control the electrode kinetics is essential to optimize the properties of $LiFePO_4$. Cyclic voltammetry (CV) is an important technique employed to study the electrochemical properties of lithium-ion battery systems [19]. Information on relevant parameters such as diffusion coefficient of lithium ion and the standard rate constant of the electron transfer process in the rate-limiting step can be obtained from the analysis of the CV profiles. Literature is replete with data on the diffusion coefficient of lithium ion in $LiFePO_4$ unlike the latter. In this study, the standard rate constants of pristine $LiFePO_4$ and the composite cathode were determined using the Klingler and Kochi equation [20], when the change in the peak-to-peak separation of the anodic and cathodic waves lie outside the range of values of the Nicholson's treatment [21] for the dimensionless parameter, Ψ. Values of these kinetic parameters determined from CV were compared with those obtained from electrochemical impedance spectroscopy (EIS).

2. EXPERIMENTAL

2.1. Materials

Iron (II) sulfate heptahydrate ($FeSO_4.7H_2O$), cobalt (II) chloride hexahydrate ($CoCl_2.6H_2O$), sodium borohydride ($NaBH_4$, 98%), trisodiumcitrate dihydrate ($Na_3C_6H_5O_7.2H_2O$, 99%), ethanol

(C_2H_6O, absolute), acetone (C_3H_6O, 99.8 %), aniline ($C_6H_5NH_2$, 99%), poly(4-styrenesulfonic acid, 18% w/v aqueous solution), ammonium persulfate ($(NH_4)_2S_2O_8$), nitric acid (HNO_3, 65%), N-methyl-2-pyrrolidone, lithium ribbon (0.75 mm thick, 45 mm wide, 99.9%) were all purchased from Sigma-Aldrich. Sulfuric acid (H_2SO_4, 98%) was purchased from Kimix; hydrochloric acid (HCl, 37%) was purchased from Fluka; poly(vinylidene fluoride), carbon black, $LiFePO_4$ powder, 1 M stock electrolyte solution of $LiPF_6$ in 1:1 v/v ethylene carbonate (EC)-dimethyl carbonate (DMC), aluminium foil, positive and negative electrode casings, springs, spacers and celgard separators were obtained from MTI Corporation. Home grown carbon nanotubes (CNTs; diameter of 40-200 nm and length up to 20 µm; synthesized according to [22]) were used. Water obtained from a Millipore Milli-Q purification system with resistivity 18.2 MΩ cm, was used to prepare all aqueous solutions. Before use, all the glassware was cleaned with freshly prepared aqua regia (HNO_3: HCl) 1:3, % v/v), rinsed thoroughly with water, and dried.

2.2. Synthesis of $LiFePO_4$/10% FeCoCNT-PA composite

Firstly, CNTs were purified according to the procedure developed by Liu *et al* [23]. Briefly, 50 mg of CNT was added to 100 mL of an acid mixture of 3:1 concentrated sulphuric acid and concentrated nitric acid. The CNTs were sonicated in a DC200H ultrasonic cleaner (mrc) for 8 h. The purified nanotubes were centrifuged using a Mini - Plus Eppendorf: 12-place fixed-angle rotor for 1.5 – 2.0 mL tubes (F-45-12-11) of radius 6 cm at 14100 relative centrifugal force (RCF) and washed with water until the pH tested neutral. The washed CNTs were vacuum dried overnight at 50 ºC.

Functionalisation of the purified CNTs with FeCo nanoparticles (to obtain FeCoCNT) was achieved through the reductive precipitation of metal salts within a CNT suspension according to the modified procedure [24]: 1 mg CNT and 2 mL of 1% sodium citrate (complexant) were added into a 100 mL flask containing 0.05 M aqueous mixture of $FeSO_4.7H_2O$ and $CoCl_2.6H_2O$. The resultant mixture was ultrasonicated for 2 h at room temperature followed by careful addition of 0.6 g $NaBH_4$. This was allowed to stir for 30 min followed by filtration through 0.2 µm Nylon 6.6 membrane filter paper. To get rid of the excess borohydride, the particles were washed with copious amounts of water and rinsed with ethanol and acetone, in that order. The washed particles were vacuum dried overnight at 50 ºC.

Chemically synthesized FeCoCNT/polyaniline composites were obtained by a simultaneous chemical polymerization of aniline monomer in the presence of acidic suspension of FeCoCNT. 0.05 mg FeCoCNT in 50 mL of 1 M HCl was sonicated for 30 min; then 1 mL distilled aniline monomer and poly (4-styrenesulfonic acid) dopant (monomer to dopant ratio of 4:1) were dissolved in the suspension and stirred magnetically in ice bath for 30 min. 0.5 g of $(NH_4)_2S_2O_8$ (ammonium persulfate) which acts as an oxidant, was slowly added into the above suspension. The mixture was reacted for 30 min at 0-5 °C. The dark suspension became green which is an indication of the beginning of polymerisation reaction of aniline monomer. Polymerisation was carried out at the specified temperature for 24 h. The composite was obtained by filtering and rinsing the reaction mixture several times with distilled water and ethanol, resulting in the conductive emeraldine salt form

of FeCoCNT/polyaniline composite. Finally, the dark-green composite was dried at 60 °C for 24 h under vacuum. This composite will be subsequently referred to as FeCoCNT-PA.

$LiFePO_4$/10% FeCoCNT-PA composite was prepared through a reported procedure [25]. Accordingly, FeCoCNT-PA was dispersed in water under short sonication in ultrasonic bath. To this dispersion, $LiFePO_4$ powder was added (in a proportion of 10% of FeCoCNT-PA in the mixture) and stirred overnight. The suspension was subsequently evaporated to dryness. Scheme 1 presents a simulative view of the whole procedure:

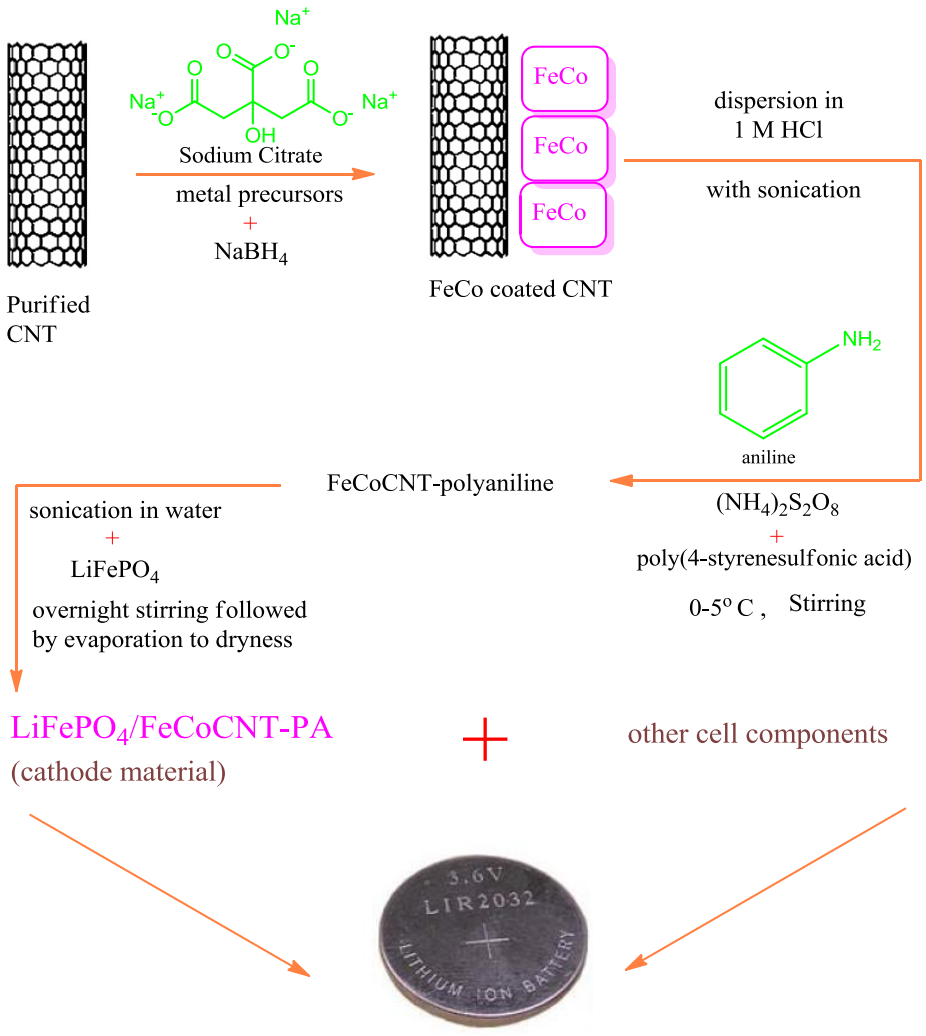

Scheme 1. Simulative view of the synthesis of $LiFePO_4$/FeCoCNT-PA and cell assembly.

2.3. Characterisation

The surface morphology and size distribution of the nanomaterials were examined through SEM and TEM images obtained from ZEISS ULTRA SS (Germany) Field Emission Scanning Microscope; JEOL JSM-7500F Scanning Electron Microscope (US) and Tecnai G2 F20X-Twin MAT 200 kV Field Emission Transmission Electron Microscope (FEI, Eindhoven, Netherlands). The X-ray

diffraction (XRD) patterns were recorded using a D8 Advance diffractometer (BRUKER AXS, Germany) with Cu Kα radiation (λ=1.5406Å) at 40 kV and 40 mA. The scan data were collected in the 2θ range from 10–80º with step size of 0.028º.

2.4. Cell assembly and electrochemical measurements

The LIR 2032 coin cells (Scheme 1) of Li ｜ $LiPF_6$ (EC: DMC=1:1 in volume ratio) ｜active Li cathode were assembled according to the following steps: first, the working cathode was prepared by mixing 80% of the active material with 10% carbon black and 10% poly (vinylidene fluoride) in N-methyl-2-pyrrolidone. The slurry was spread uniformly on a thin aluminium foil and dried in vacuum at 120 ºC for 12 h. The coated aluminium foil was roll-pressed and punched out to the required dimension with a punching machine. A metal lithium ribbon (permanently kept in the glove box) was used as anode and punched to the same dimension as the cathode. Together with the other cell components (positive and negative electrode casings, spring, spacer, polypropylene micro-porous film (celgard) separator and the electrolyte), the LIR 2032 coin cells were assembled in a dry argon-filled LABSTAR MBRAUN glove box in which the oxygen and water contents were maintained below 1 ppm, and crimp-sealed for further electrochemical studies.

Cyclic voltammetry (CV), EIS and galvanostatic charge/discharge studies were carried out using the crimp-sealed LIR 2032 laboratory coin cells. CV and EIS measurements were conducted on Zahner IM6ex (Germany) Electrochemical workstation. A Potential range of: 2.3 - 4. 0 V and 0.1- 0.8 mV/s scan rates were used for CV while EIS measurements were recorded at a formal potential of 3.4 V and perturbation amplitude of 5 mV within the frequency range of 100 mHz – 100 kHz. Charge/discharge data were recorded from MTI 8 Channels Battery Analyser between 3.0 - 4.0 V at 0.1 C rates. All potentials were measured against Li/Li^+.

3. RESULTS AND DISCUSSION

3.1. Structural and morphological analysis

FeCo bimetallic nanoparticles of 35-50 nm diameters were attached to CNTs (FeCoCNT) according to Scheme 1 above. Fig. 1 represents the TEM micrograph of FeCoCNT:

The morphologies of bimetallic FeCo, CNTs and FeCo-derivatised CNTs are depicted in the SEM micrographs in Figs. 2 - 4. The successful fabrication of the FeCoCNT composite through the above scheme is a prelude to the formation of a strong 3D nano-network of CNT and adjacent $LiFePO_4$ particles which through a kinetic synergy with polyaniline nanomaterials, enhances the electrochemical performance of $LiFePO_4$ [18, 26]. As shown in Fig. 4, the morphology of the FeCoCNT enables faster and facile lithium ion transport within the composite cathode material.

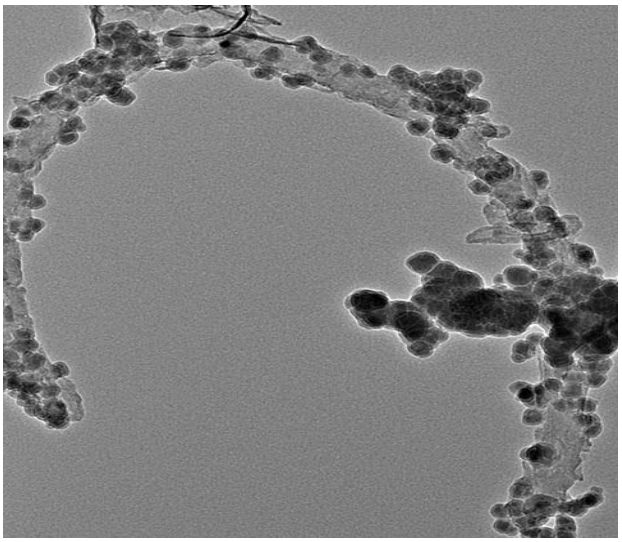

Figure 1. HRTEM image of FeCo-functionalised CNTs.

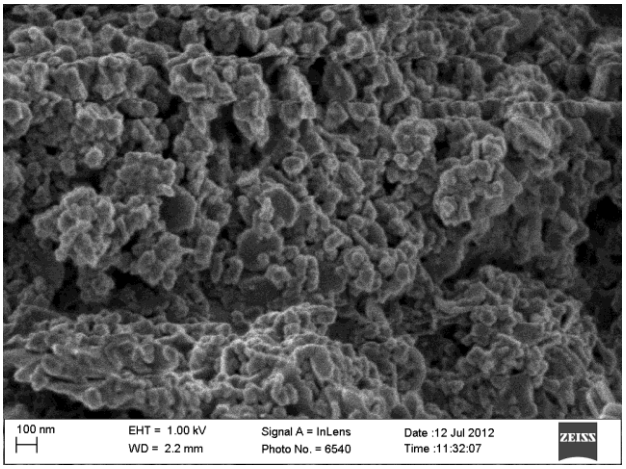

Figure 2. SEM image of FeCo nanoparticles.

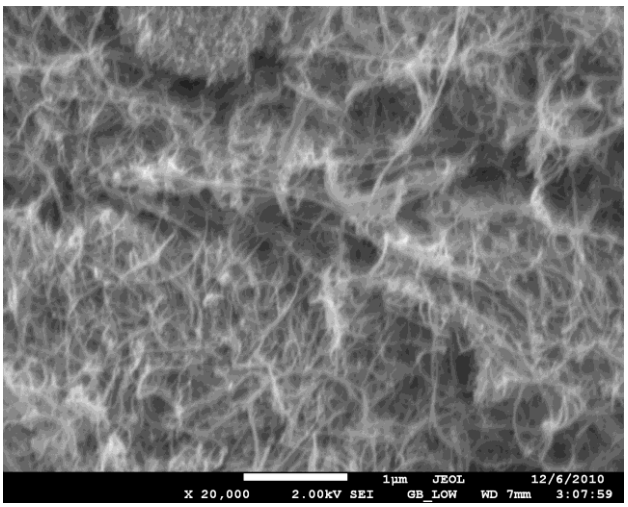

Figure 3. SEM image of CNTs.

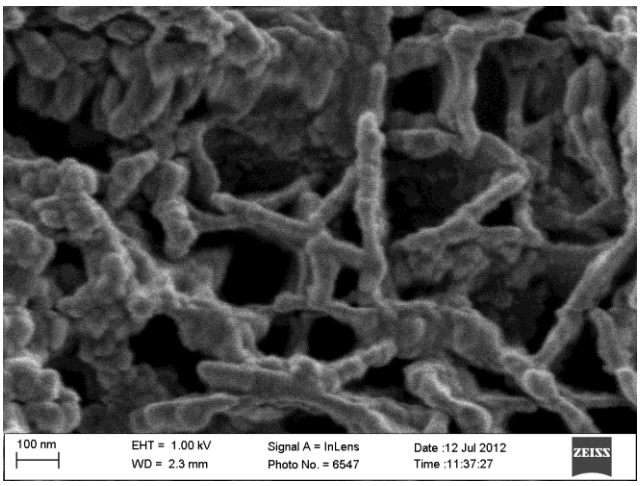

Figure 4. SEM image of FeCo-CNT.

Fig. 5 shows the XRD patterns of composite $LiFePO_4$/10% FeCoCNT-PA and pristine $LiFePO_4$:

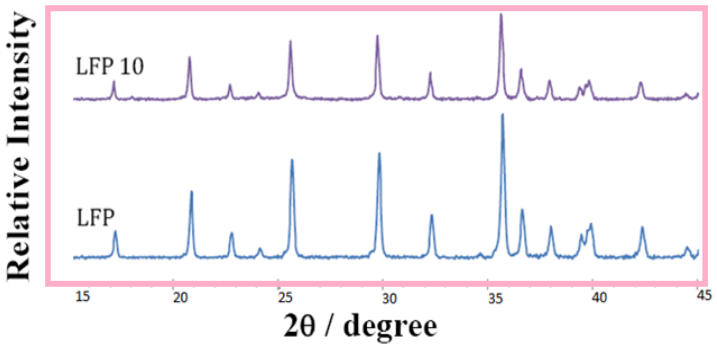

Figure 5. XRD patterns of composite $LiFePO_4$/10% FeCoCNT-PA and pristine $LiFePO_4$.

All the diffraction peaks are indexed to a single phase of an orthorhombic olivine-type structure with space group *Pnma* according to ICDD File No: 83-2092. The lattice parameters as shown in Table 1, were calculated based on the XRD patterns and are found to be in good agreement with the standard values.

Table 1. Lattice Parameters of composite $LiFePO_4$/10% FeCoCNT-PA and pristine $LiFePO_4$

Cathode	*a*/Å	*b*/Å	*c*/Å	*Cell volume*/Å^3
Composite	10.31695	6.00113	4.68643	290.1527
Pristine	10.29123	5.99274	4.67025	288.0271

Compared with the pristine $LiFePO_4$, the presence of the conductive additives in the composite $LiFePO_4$/10% FeCoCNT-PA cathode resulted in a slight increase in the lattice constants as well as expansion of the cell volume. This expansion is expected to provide more space for lithium ion intercalation/de-intercalation [27-28].

3.2. Electrochemical characterisation

Fig. 6 shows the cyclic voltammograms of $LiFePO_4$/10% FeCoCNT-PA and pristine $LiFePO_4$.

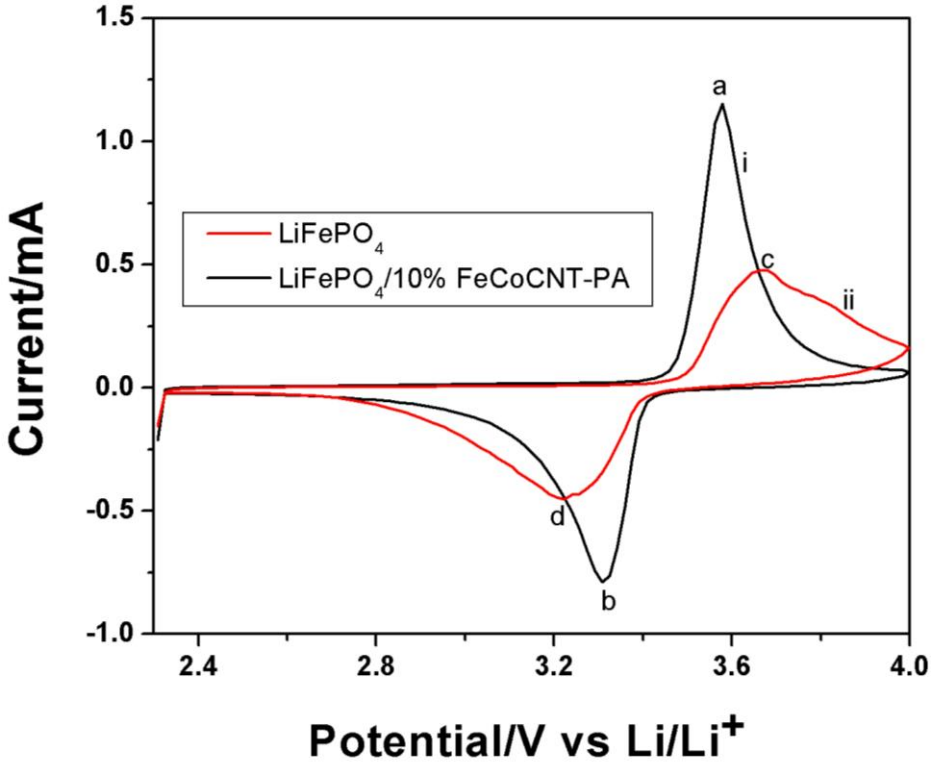

Figure 6. Comparative cyclic voltammograms of (i) $LiFePO_4$/10% FeCoCNT-PA and (ii) pristine $LiFePO_4$ in 1 M $LiPF_6$ containing 1:1 v/v ethylene carbonate – dimethyl carbonate solvent mixture. Scan rate 0.1 mV/s (voltage range: 2.3 – 4.0 V).

The cyclic voltammograms are characterised by a well-defined pair of redox peaks which are associated with the electrochemical lithium ion deinsertion/insertion within the octahedral sites of the $LiFePO_4$ structure upon the two phase oxidation/reduction of Fe^{2+}/Fe^{3+} redox couple [6, 29-30]. However, the shapes of the voltammograms show that the pristine $LiFePO_4$ cathode with diminished and broadened peaks revealed more sluggish lithium deinsertion/insertion behaviour. The sharp peaks of $LiFePO_4$/10% FeCoCNT-PA composite cathode indicate a more facile lithium ion transfer resulting in better reaction kinetics. Again, the peak to peak separation in $LiFePO_4$/10% FeCoCNT-PA (ΔE_p = E_{pa}- E_{pc} = 270 mV) is less than that of the pristine $LiFePO_4$ (ΔE_p = 441 mV) which suggests better electrochemical reversibility in the former than in the latter.

Analysis of voltammogram *i*, which is due to $LiFePO_4$/10% FeCoCNT-PA, gave an anodic peak, *a* (I_{pa} = 1.15 mA, E_{pa} = 3.58 V) and a cathodic peak, *b*, (I_{pc} = 0.79 mA, E_{pc} = 3.31 V) at a formal potential, $\Delta E^{0`} = (E_{pa} + E_{pc})/2$ = 3.44 V. This formal potential value has been reported [31-32] and is synonymous with the potential at the point of inflexion on the flat plateau at 3.45 V, observed during battery cycling experiments, where lithium deinsertion/insertion occurs as a two-phase process. Peak *a*, corresponds to the delithiation of $LiFePO_4$ to the charged state of the functioning battery, $FePO_4$. Complete extraction of lithium corresponds to a theoretical specific capacity of 170 mAh/g [29]. Conversely, peak *b* arose from the lithiation of the isostructural $FePO_4$ under the electrochemically reducing conditions. Voltammogram *ii* showed that the pristine $LiFePO_4$ gave an anodic peak at *c* (I_{pa} = 0.48 mA; E_{pa} = 3.66 V) and a cathodic peak, *d* (I_{pc} = 0.45 mA; E_{pc} = 3.22 V) at a formal potential, $\Delta E^{0`}$ = 3.44 V. Peak *c* corresponds to lithium deinsertion as peak *a* while peak *d* involves the insertion of lithium as peak *b*.

Charge/discharge capacities obtained from the integrated area under the anodic peak at the scan rate of 0.1 mV/s indicate that the composite $LiFePO_4$/10% FeCoCNT-PA cathode exhibited a charge capacity of 148 mAh/g and a discharge capacity of 134 mAh/g for the insertion of lithium and reduction of Fe^{3+} to Fe^{2+} upon integration of the cathodic peak; thus, giving a charge/discharge reversibility of 91%. Both capacities were found to be well within the range of reported values using data obtained from cyclic voltammetry [19, 25, 31]. The effect of potential scan rate on the cyclic voltammogram of the composite cathode is as shown in Fig. 7. Although the wave shapes of the anodic and cathodic peaks were almost symmetrical, the difference between the peak potentials, ΔE_p, was observed to increase with increasing scan rate, ν, and calculated to be 421 ± 121 mV which is higher than the 59 mV expected for an ideal Nernstian process; and shows that there are some kinetic limitations during the electrochemical processes [33-34].

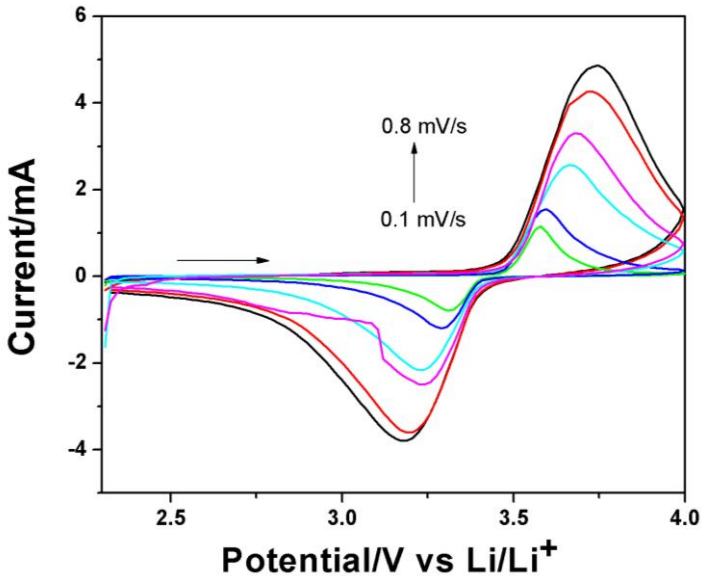

Figure 7. The effect of potential scan rate on the cyclic voltammograms of $LiFePO_4$/10% FeCoCNT-PA in 1 M $LiPF_6$ containing 1:1 v/v ethylene carbonate – dimethyl carbonate solvent mixture between 0.1 – 0.8 mV/s. Voltage range: 2.3 – 4.0 V.

Such behaviour is attributed to lithium ion interfacial charge transfer as well as other electrochemical processes involved in the diffusion of lithium ions in a solid phase and electron jumping across a poorly or fairly conducting compound [35-36]. Thus, the ΔE_p, unlike in an ideal reversible condition, is dependent on ν. Moreover, the peak intensities follow the linear law, $I_p = f(\nu)$ with the ratio of peak currents, (I_{pa}/I_{pc}) calculated to be 1.29 ± 0.1. Furthermore, considering the fact that quasi-reversible electron transfer processes behave reversibly at low scan rates and irreversibly at high scan rates [33] as depicted in Figs 8 (i) and (ii):

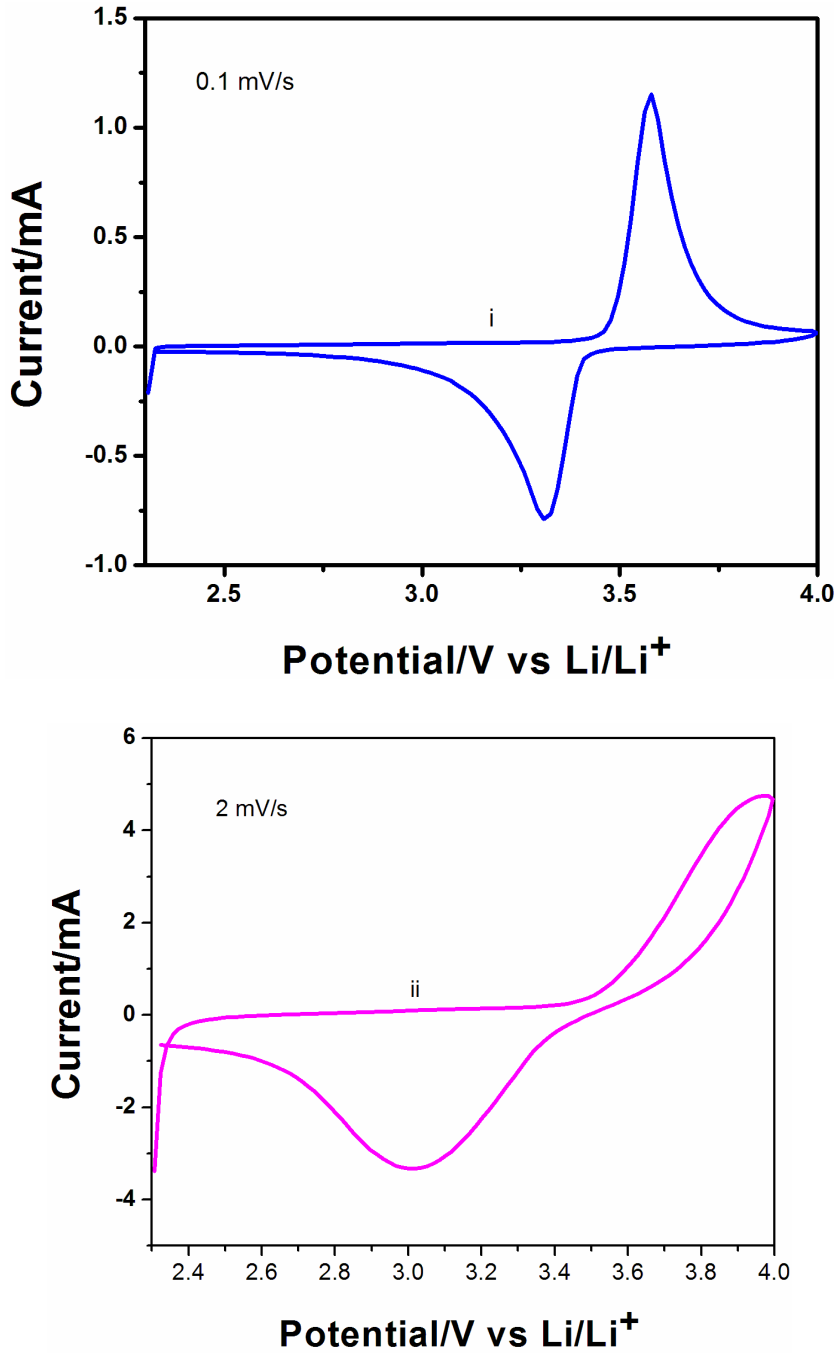

Figure 8. Comparative cyclic voltammograms of $LiFePO_4$/10% FeCoCNT-PA at (i) 0.1 and (ii) 2 mV/s scan rates.

- For 0.1 and 2 mV/s scan rates, it therefore suggests that the Fe^{2+}/Fe^{3+} redox reaction in the $LiFePO_4$/10% FeCoCNT-PA electrochemical system under study is quasi-reversible. This phenomenon was also reported by other researchers [31-32, 37] and equally observed in the behaviour of the pristine $LiFePO_4$ (Fig. 9). However, the degree of irreversibility is higher in the pristine electrode (ΔE_p = 704 ± 220 mV; formal potential = 3.45 ± 0.004 V; I_{pa}/I_{pc} = 1.3 ± 0.1).

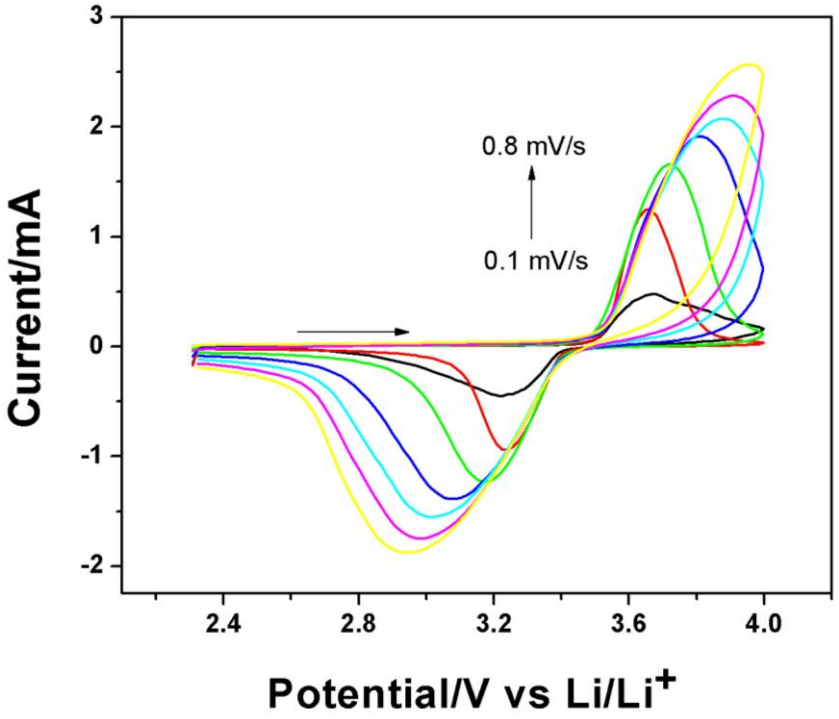

Figure 9. The effect of potential scan rate on the cyclic voltammograms of pristine $LiFePO_4$ in 1 M $LiPF_6$ containing 1:1 v/v ethylene carbonate – dimethyl carbonate solvent mixture between 0.1 – 0.8 mV/s. Voltage range: 2.3 – 4.0 V.

The improvement of the composite electrode over the pristine electrode is ascribed to a synergistic kinetic-effect of the conductive polyaniline and carbon nanotubes additives in the former which enhances its elctrochemical activity. Polyaniline serves as a host for lithium ion intercalation and extraction and provides good electronic contact between the $LiFePO_4$ particles and the current collector through an overlap of the electrochemically active energies of the conductive polymer and that of the working redox couple of the carbon- coated oxide insertion compound, $LiFePO_4$ [18]. On the other hand, the nanoscale networking with carbon nanotubes enhances the mobility of electrons between the adjacent $LiFePO_4$ particles during the lithiation/delithiation process in such a way that the nanotubes interlace adjacent $LiFePO_4$ nanoparticles together to form a 3D network wiring without blocking the lithium ion transport [26].

Log-log plots of peak current versus scan rate for the composite electrode shows that the diffusion of lithium ion on the electrode surface is the rate- limiting step. This was confirmed by the slope values of 0.67 and 0.64 obtained for the anodic and cathodic waves, respectively.

Electrochemical profiles of this nature for diffusion-controlled processes are known to give slopes of 0.5 [38]. The slight deviations from this value is however, as a result of the contributions of adsorption processes at the metal/electrolyte interface due to the presence of the FeCo bimetallic nanoparticles that were used to functionalise the nanotubes; and charging of electronically conducting polymers as a result of polyaniline film on the electrode surface [39-41]. Hence, the Fe^{2+}/Fe^{3+} redox process upon deinsertion/insertion of lithium in the composite $LiFePO_4$/10% FeCoCNT-PA cathode was largely due to diffusion. To buttress this point, log-log plots of the pristine $LiFePO_4$ gave slopes that were approximately = 0.5, indicating the absence of adsorption processes emanating from the conductive additives. The diffusion coefficient, *D*, calculated from the Randles-Sevčik plot was found to be 1 x 10^{-9} cm^2/s for the composite electrode and is consistent with those measured by Liu *et al* [14] but about three orders of magnitude higher than values reported by Fey *et al* [42-43]; and two orders of magnitude higher than the pristine $LiFePO_4$ which was calculated to be 4.81 x 10^{-11} cm^2/s. This difference is ascribed to the synergistic kinetic effects of the conductive additives in the composite cathode as previously discussed.

The redox properties of the pristine and composite electrodes were further interrogated by determining the rate constant of the electron transfer process in the rate-limiting step. The standard rate constant, k_s of an uncomplicated quasi-reversible electrochemical reaction and the scan rate, ν, are governed by the Nicholson's equation [21]:

$$\Psi = k_s \left[\pi D n \nu F / (RT) \right]^{-1/2} \quad (1)$$

where Ψ is the charge transfer parameter. The other symbols have their usual meanings. Equation (1) is applicable when (ΔE_p x *n*) values do not exceed 212 mV and under such conditions, the least value of the dimensionless parameter, Ψ that could be obtained is 0.1 [21, 44]. Therefore, when the measured ΔE_p values lie outside the range of Ψ values of the Nicholson's treatment, the Klingler and Kochi equation [20] can be used to calculate k_s from CV curves:

$$k_s = 2.18 \left(\frac{D \beta n F \nu}{RT} \right)^{1/2} \exp\left(- \frac{\beta^2 n F}{RT} (E_{pa} - E_{pc}) \right) \quad (2)$$

where β is the transfer coefficient for the electrode process [20] and represented by α (Table 2). The summary of the calculated kinetic parameters using the above relation is shown in Table 2:

Table 2. Electrochemical kinetic parameters of composite $LiFePO_4$/10% FeCoCNT-PA and pristine $LiFePO_4$ obtained from cyclic voltammetry at 298 K.

Cathode	D/cm^2 s^{-1}	Q/C	Γ/mol cm^{-2}	α	k_s/cm s^{-1}	Conductance/S
Composite	1.0 x 10^{-9}	1.95	1.005 x 10^{-5}	0.3	7.05 x 10^{-7}	1.83 x 10^{-2}
Pristine	4.81 x 10^{-11}	1.62	8.361 x 10^{-6}	0.1	2.68 x 10^{-7}	8.21 x 10^{-3}

The values of the parameters in Table 2 show that electrode reactions are kinetically more facile in the modified cathode system than in the unmodified one as a result of the presence of the conductive additives in the former. The conductance profile of the redox states of the pristine and composite electrodes were determined from the CV data (Figs. 7 and 9) by applying the classical Ohm's relation to multiple potential scan rate cyclic voltammetry [45]. The composite cathode gave higher conductance values (Table 2) as a result of the conductive additives present. This observation is in good agreement with reported values from cyclic voltammetry [45].

EIS tests were conducted to evaluate the interfacial properties as well as the Li^+ migration dynamics of the composite and pristine electrodes. The Nyquist plots are presented in Fig. 10.

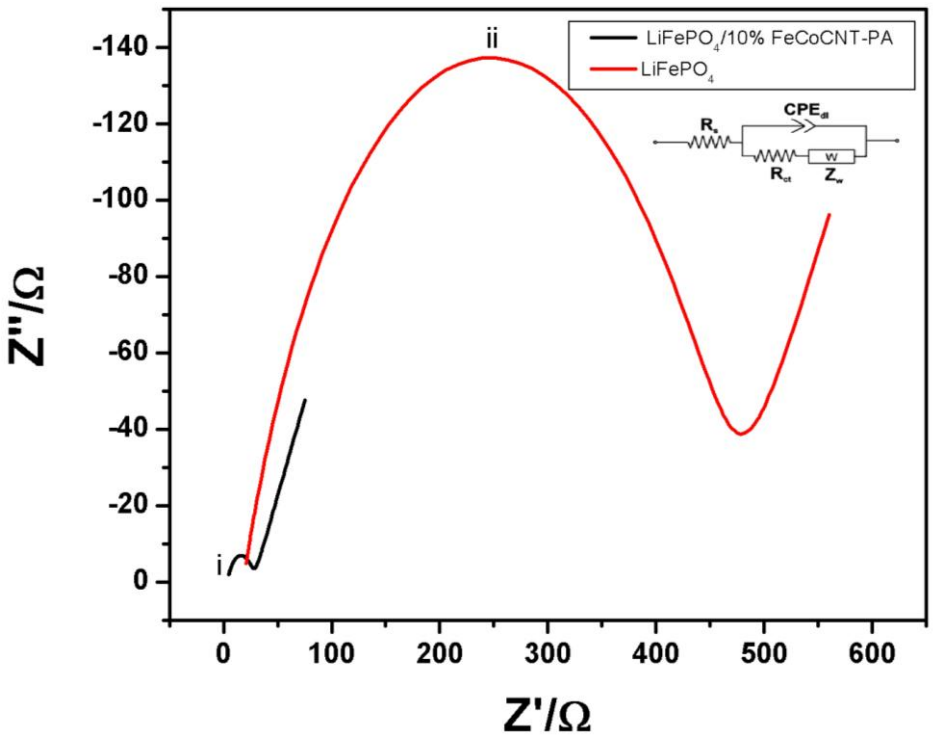

Figure 10. Comparative Nyquist plots of (i) $LiFePO_4$/10% FeCoCNT-PA and (ii) pristine $LiFePO_4$ at formal potential of 3.4 V vs. Li/Li^+ and perturbation amplitude of 5 mV.

Each plot gave a well-defined, single semi-circle at high frequency and an inclined line at low frequency attributed to Warburg impedance associated with lithium ion diffusion in the bulk of the electrode. This is an indication that during lithium deinsertion/insertion, the kinetics of the electrode process is controlled by the diffusion process in the low frequency region and by the charge transfer in the high frequency region [29, 46-48]. An intercept of the semi-circle with the Z'-axis in the very high frequency region identifies the Ohmic resistance (R_s) of the electrolyte and electrodes. The diameter of the semicircle at high frequency region on the Z'-axis is related to the charge transfer resistance (R_{ct}) which controls the transfer kinetics at the electrode interface. Extrapolation of the semi-circle to lower frequencies gives an intercept corresponding to $R_s + R_{ct}$ from which the value of R_{ct} was determined by subtracting R_s value. Impedance parameters were obtained by fitting from a modified Randles

equivalent electrical circuit (inset). The constant phase element (CPE) models the double layer capacitance (C_d) which is due to surface roughness. The time constant (τ); exchange current (I_o), a measure of the rate of exchange of charge between oxidized and reduced species at any equilibrium potential without net overall change [49], and heterogeneous rate constant of electron transfer (k_{et}) were calculated according to [50-52]. A marked decrease in semi-circle ($R_{ct\text{-}pristine}$ = 450.7 Ω; $R_{ct\text{-}composite}$ = 24.57 Ω) shows that the composite electrode has better conducting properties with enhanced electron transfer mediation than the pristine electrode. This observation is corroborated by the Bode phase-impedance plots (Fig. 11) where the pristine electrode exhibited higher impedance to electron transfer than the composite electrode as evidenced by the impedance and phase angle values (pristine: 572.7 Ω and 10.4°; composite: 98.86 Ω and 34.7°) at low frequency regimes where disturbances to the equilibrium positions of the systems are minimal. This lends credence to the fact that facile electrode kinetics takes place on the composite cathode than on the unmodified $LiFePO_4$.

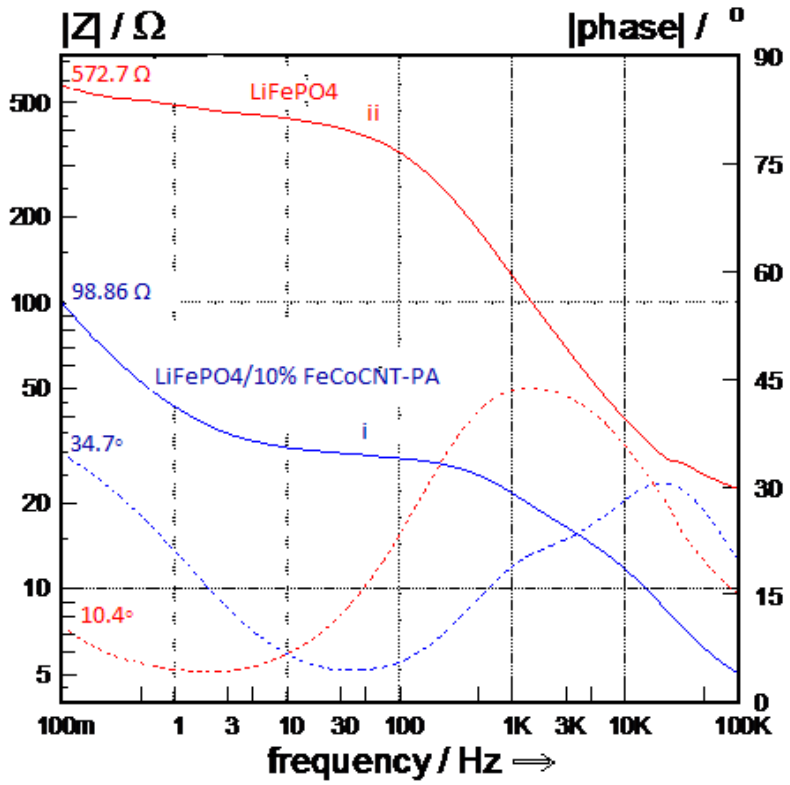

Figure 11. Comparative Bode phase-impedance diagrams of (i) $LiFePO_4$/10% FeCoCNT-PA and (ii) pristine $LiFePO_4$ at 3.4 V vs. Li/Li^+ and perturbation amplitude of 5 mV.

It has been established that the diffusion of lithium ion within the electrode is the rate-limiting step [35]. The exploitation of the Warburg domain allows determination of the kinetics of this limiting process. From the plots of Z_{re} vs. $\omega^{-½}$ (Z_{re} = real impedance; ω = angular frequency) as shown in Figs. 12 and 13 according to [50], the diffusion coefficient, D was calculated (Table 3) using the relation:

$$D = \left(\frac{\sqrt{2}\ RT}{\sigma n^2 F^2 AC} \right)^2 \quad (3)$$

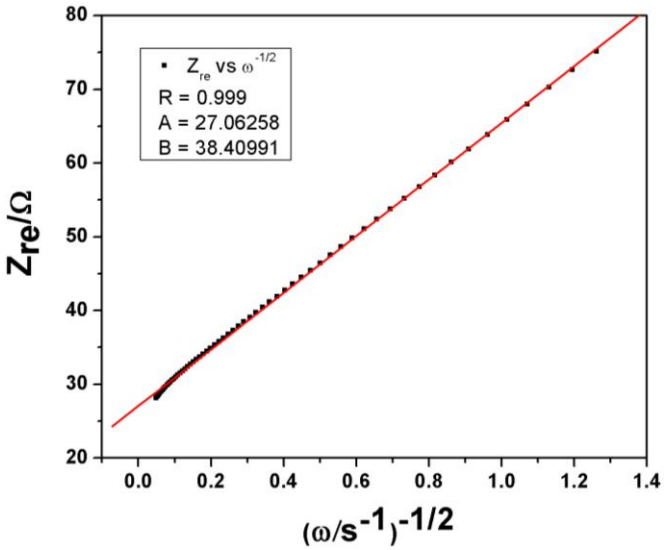

Figure 12. The plot of Z_{re} vs $\omega^{-½}$ for composite $LiFePO_4$/10% FeCoCNT-PA cathode.

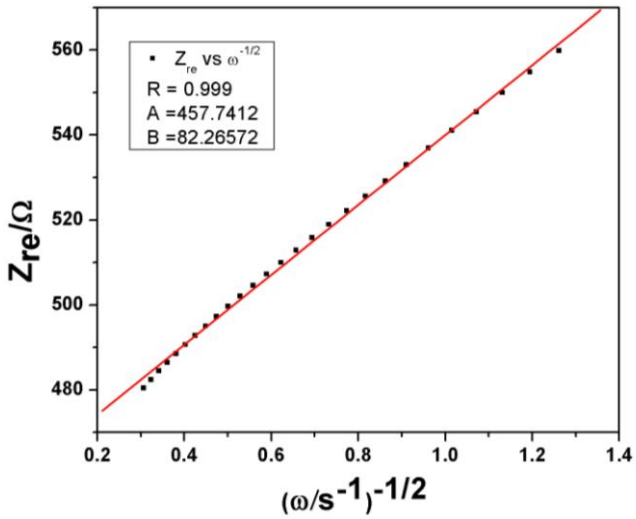

Figure 13. The plot of Z_{re} vs. $\omega^{-½}$ for pristine $LiFePO_4$.

Table 3. Kinetic parameters of composite $LiFePO_4$/10% FeCoCNT-PA and pristine $LiFePO_4$ obtained from electrochemical impedance spectroscopy at 298 K.

Cathode	τ/s rad^{-1}	R_{ct}/Ω	I_o/A	k_{et}/cm s^{-1}	σ/Ω s$^{-1/2}$	D/cm^2 s^{-1}
Composite	6.43 x 10^{-5}	24.57	1.045 x 10^{-3}	2.36 x 10^{-7}	38.41	4.57 x 10^{-14}
Pristine	9.76 x 10^{-4}	450.7	5.70 x 10^{-5}	1.20 x 10^{-8}	82.27	9.97 x 10^{-15}

It is evident from Table 3 that the composite, with lower value of the Warburg coefficient, σ, has a higher *D* value thus confirming the earlier observations that faster lithium ion diffusion takes place on the modified electrode than on the pristine cathode due to the presence of the conductive additives. Regrettably, the calculated values of the diffusion coefficients could not be compared with those from literature, where the above procedure was employed, as wrong equations for *D* were used [10, 53-55]. The values of *D* from the two different techniques (CV: $D_{composite}$ = 1 x 10^{-9}; $D_{pristine}$ = 4.81 x 10^{-11}; and EIS: $D_{composite}$ = 4.57 x 10^{-14}; $D_{pristine}$ = 9.97 x 10^{-15}), however, show significant discrepancies due to the limitations involved in each measurement. This phenomenon has been reported [14, 46, 56]. The conductive additives facilitated lithium ion diffusivity thereby increasing the kinetics of the phase transformation between the charged phase and discharged phase. The rate constant of electron transfer calculated from both techniques (CV: $k_{composite}$ = 7.05 x 10^{-7}; $k_{pristine}$ = 2.68 x 10^{-7} and EIS: $k_{composite}$ = 2.36 x 10^{-7}; $k_{pristine}$ = 1.20 x 10^{-8}) revealed complementary results from both techniques and showed the composite cathode having values of about an order of magnitude higher than the pristine $LiFePO_4$ electrode. This was made possible by the kinetic synergistic effects of the conductive FeCo-derivatised CNTs and polyaniline nanomaterials that were present in the composite cathode system.

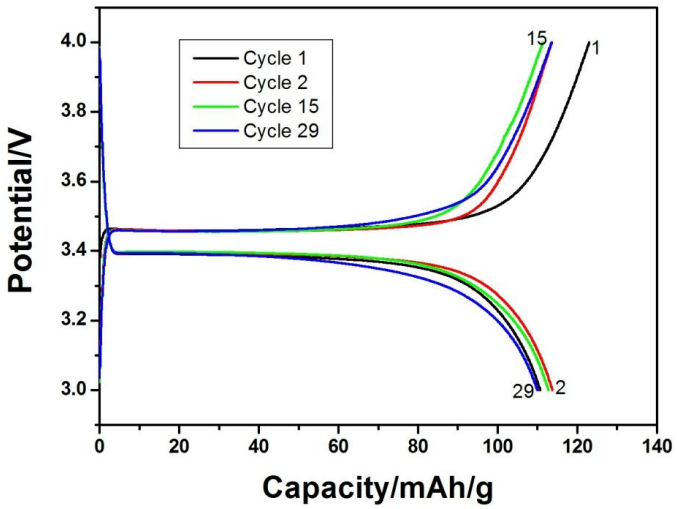

Figure 14. Charge/discharge curves of composite $LiFePO_4$/10% FeCoCNT-PA at 0.1 C rates for the 1^{st}, 2^{nd} 15^{th} and 29^{th} cycles.

The galvanostatic charge-discharge performance of the composite and pristine electrodes was determined at 0.1 C rates as shown in Figs. 14 - 16:

A flat charge/discharge voltage plateau was observed for both the pristine $LiFePO_4$ and composite $LiFePO_4$/10% FeCoCNT-PA systems between 3.4 V - 3.5 V ranges which is consistent with the CV formal potential obtained at around 3.44 V and typical of a well-defined $LiFePO_4$ olivine structure indicating the two-phase nature of lithium deinsertion/insertion between $LiFePO_4$ and $FePO_4$ [6]. As shown in Fig. 16 for the 15^{th} cycle, the composite cathode exhibited longer and flatter voltage profile than the pristine with charge and discharge capacities of 111.41 and 112.78 mAh/g,

respectively. Chen *et al* reported similar capacities at the investigated current rate [53]. The pristine electrode, with a broader and shorter voltage plateau, gave charge and discharge capacities at 98.88 mAh/g and 91.29 mAh/g.

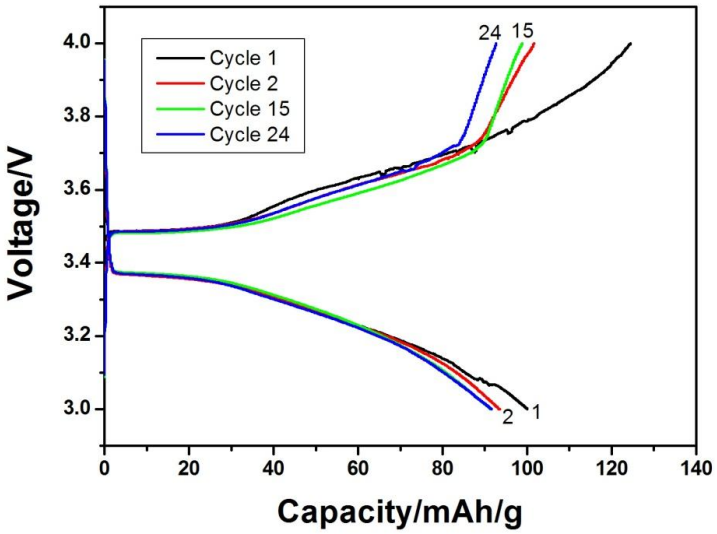

Figure 15. Charge/discharge curves of pristine $LiFePO_4$ at 0.1 C rates for the 1st, 2nd 15th and 24th cycles**.**

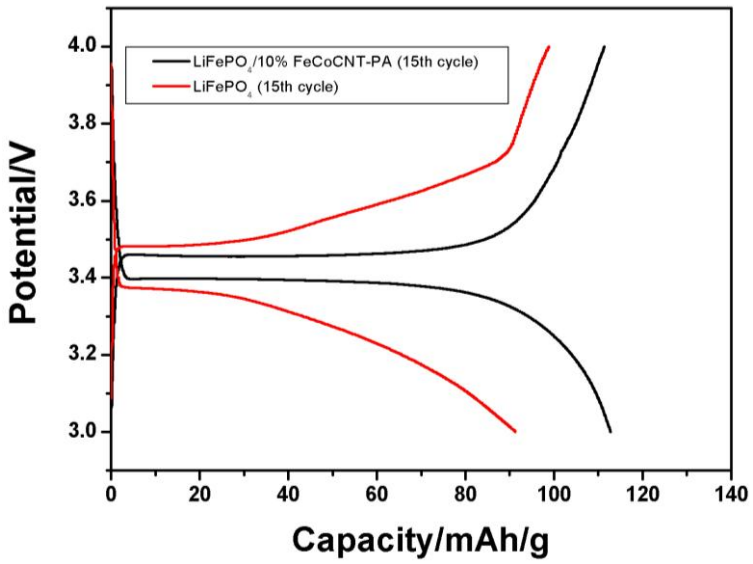

Figure 16. Comparative charge/discharge curves of composite $LiFePO_4$/10% FeCoCNT-PA and pristine $LiFePO_4$ at 0.1 C rates for the 15th cycle.

Fig. 17 shows the profiles of the discharge capacities for the pristine and composite cathodes versus the cycle numbers.

As observed from Fig. 17, the composite cathode showed very little capacity attenuation. This behaviour culminated in a capacity retention of 99.72%, Coulombic efficiency of 90% and 10% loss in capacity which is attributed to current ineffciencies during cycling. The Coulombic efficiency is in good agreement with the charge/discharge reversibility of 91% obtained from CV measurements. The pristine electrode on the other hand was found to have a capacity retention of 89.61% , 80.36 % Coulombic efficiency and capacity loss of 19.64 %.

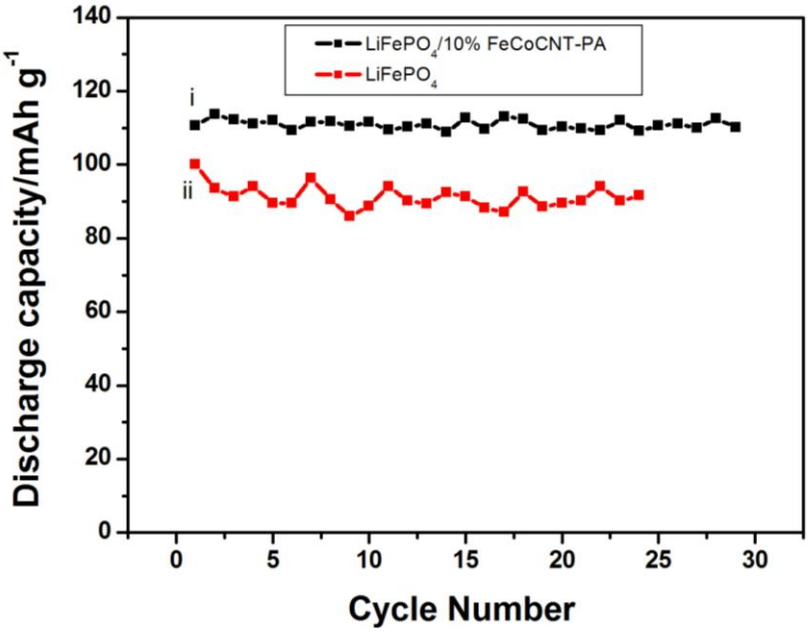

Figure 17. Discharge capacity vs cycle number profiles at 0.1C for (i) the first 29 cycles of composite $LiFePO_4$/10% FeCoCNT-PA and (ii) the first 24 cycles of pristine $LiFePO_4$.

4. CONCLUSION

Novel lithium ion battery cathode based on $LiFePO_4$/10%FeCoCNT-PA composite was developed in this study. The composite cathode gave better intercalation kinetics and electrochemical performance than the pristine electrode. This was confirmed from the voltammetric, impedimetric and galvanostatic charge/discharge data. The rate constant of electron transfer calculated from cyclic voltammetry using the Klingler and Kochi equation, as well as electrochemical impedance spectroscopy revealed complementary results from both techniques and showed the composite cathode having values of about an order of magnitude higher than the pristine $LiFePO_4$ electrode. This was made possible by the kinetic synergistic effects of the conductive FeCo-derivatised CNTs and polyaniline nanomaterials that were present in the composite cathode system. Due to this same synergy, values of diffusion coefficients calculated from CV showed the performance of the composite electrode to be about two orders of magnitude higher than the pristine. The charge and discharge capacities of the composite cathode at 0.1 mV/s scan rate combined to give a reversible capacity of 91% which is consistent with the Coulombic efficiency of 90% calculated from galvanostatic

charge/discharge experiments for the first cycle at 0.1 C rates. The novel electrode exhibited excellent cyclability after 20 cycles with a capacity retention of 99.72%.

ACKNOWLEDGEMENT
National Research Foundation (NRF) of South Africa and Council for Scientific and Industrial Research (CSIR), Pretoria, South Africa are gratefully acknowledged.

References

1. M. Armand and J.M. Tarascon, *Nature*, 451 (2008) 652
2. A.S. Arico, P. Bruce, B. Scrosati, J.-M. Tarascon and W.V. Schalkwijk, *Nature Materials*, 4 (2005) 366
3. D. Aurbach, B. Markovsky, G. Salitra, E. Markevich, Y. Talyossef, M. Koltypin, L. Nazar, B. Ellis and D. Kovacheva, *J. Power Sources*, 165 (2007) 491
4. M. Broussely, P. Biensan and B. Simon, *Electrochim. Acta*, 45 (1999) 3
5. G.R. Dahlin and K.E. Strom, *Lithium Batteries: Research, Technology and Applications*, Nova Science Publishers, Inc. New York (2010)
6. A.K. Padhi, K.S. Nanjundaswamy and J.B. Goodenough, *J. Electrochem. Soc.*, 144 (1997) 1188
7. P.S. Herle, B. Ellis, N. Coombs and L.F. Nazar, *Nature Materials* 3 (2004) 147
8. C. Delacourt, L. Laffont, R. Bouchet, C. Wurm, J.-B. Leriche, M. Morcrette, J.M. Tarascon and C. Masquelier, *J. Electrochem Soc.*, 152 (2005) A913
9. B. Kang and G. Ceder, *Nature*, 458 (2009) 190
10. H. Liu, Q. Cao, L.J. Fu, C. Li, Y.P. Wu and H.Q. Wu, *Electrochem. Commun.*, 8 (2006) 1553
11. S.-Y. Chung, J.T. Bloking and Y.-M. Chiang, *Nature Materials*, 1 (2002) 123
12. C.R. Sides, F. Croce, V.Y. Young, C.R. Martin and B. Scrosati, *Electrochem. Solid-State Lett.*, 8 (2005) A484
13. C. Nan, J. Lu, C. Chen, Q. Peng and Y. Li, *J. Mater. Chem.*, (2011)
14. H. Liu, L.J. Fu, H.P. Zhang, J. Gao, C. Li, Y.P. Wu and H.Q. Wu, *Electrochem. Solid-State Lett.*, 9 (2006) A529
15. N. Ravet, Y. Chouinard, J.F. Magnan, S. Besner, M. Gauthier and M. Armand, *J. Power Sources*, 97-98 (2001) 503
16. G.X. Wang, S. Needham, J. Yao, J.Z. Wang, R.S. Liu and H.K. Liu, *J. Power Sources*, 159 (2006) 282
17. J. Chen and M.S. Whittingham, *Electrochem. Commun.*, 8 (2006) 855
18. Y.-H. Huang and J.B. Goodenough, *Chem. Mater.*, 20 (2008) 7237
19. D.Y.W. Yu, C. Fietzek, W. Weydanz, K. Donoue, T. Inoue, H. Kurokawa and S. Fujitani, *J. Electrochem. Soc.*, 154 (2007) A253
20. R.J. Klingler and J.K. Kochi, *J. Phys. Chem.*, 85 (1981) 1731
21. R.S. Nicholson, *Anal. Chem.*, 37 (1965) 1351
22. P. Ndungu, A. Nechaev, L. Khotseng, N. Onyegebule, W. Davids, R. Mohammed, G. Vaivars, B. Bladegroen and V. Linkov, *Int.J. Hydrogen Energy*, 33 (2008) 3102
23. J. Liu, A.G. Rinzler, H. Dai, J.H. Hafner, R.K. Bradley, P.J. Boul, A. Lu, T. Iverson, K. Shelimov, C.B. Huffman, F. Rodriguez-Macias, Y.-S. Shon, T.R. Lee, D.T. Colbert and R.E. Smalley, *Science*, 280 (1998) 1253
24. M.-S. Park, S.A. Needham, G.-X. Wang, Y.-M. Kang, J.-S. Park, S.-X. Dou and H.-K. Liu, *Chem. Mater.*, 19 (2007) 2406

25. L. Kavan, R. Bacsa, M. Tunckol, P. Serp, S.M. Zakeeruddin, F. Le Formal, M. Zukalova and M. Graetzel, *J. Power Sources*, 195 (2010) 5360
26. A.V. Murugan, T. Muraliganth, P.J. Ferreira and A. Manthiram, *Inorg. Chem.*, 48 (2009) 946
27. Y. Lu, J. Shi, Z. Guo, Q. Tong, W. Huang and B. Li, *J. Power Sources*, 194 (2009) 786
28. Y. Lin, Y. Lin, B. Zeng, G. Zhao, T. Zhou, M. Chen, Xiamei Mao, H. Lai and Z. Huang, *Int. J. Electrochem. Sci.*, 6 (2011) 6653
29. S. Franger, F. Le Cras, C. Bourbon and H. Rouault, *Electrochem. Solid-State Lett.*, 5 (2002) A231
30. J.L. Allen, T.R. Jow and J. Wolfenstine, *Chem. Mater.*, 19 (2007) 2108
31. M. Takahashi, S.-i. Tobishima, K. Takei and Y. Sakurai, *Solid State Ionics*, 148 (2002) 283
32. C.H. Mi, X.G. Zhang and H.L. Li, *J. Electroanal. Chem.*, 602 (2007) 245
33. P. Zanello, *Inorganic Electrochemistry-Theory, Practice and Application*, The Royal Society of Chemistry (2003)
34. F. Sauvage, E. Baudrin, M. Morcrette and J.M. Tarascon, *Electrochem. Solid-State Lett.*, 7 (2004) A15
35. P. He, X. Zhang, Y.-G. Wang, L. Cheng and Y.-Y. Xia, *J. Electrochem. Soc.*, 155 (2008) A144
36. F. Croce, A.D. Epifanio, J. Hassoun, A. Deptula, T. Olczac and B. Scrosati, *Electrochem. Solid-State Lett.*, 5 (2002) A47
37. S. Franger, C. Bourbon and F. Le Cras, *J. Electrochem. Soc.*, 151 (2004) A1024
38. D.K. Gosser, *Cyclic Voltammetry: Simulation and Analysis of Reaction Mechanisms*, VCH Publishers, Inc. New York (1993)
39. P.P. Prosini, M. Lisi, D. Zane and M. Pasquali, *Solid State Ionics*, 148 (2002) 45
40. M.A. Vorotyntsev and J.P. Badiali, *Electrochim. Acta*, 39 (1994) 289
41. B.E. Conway, *Electrochim. Acta*, 38 (1993) 1249
42. G.T.-K. Fey, K.-P. Huang, H.-M. Kao and W.-H. Li, *J. Power Sources*, 196 (2011) 2810
43. C.K. Park, S.B. Park, H.C. Shin, W.I. Cho and H. Jang, *Bull. Korean Chem. Soc.*, Vol. 32, (2011) 191
44. I. Lavagnini, R. Antiochia and F. Magno, *Electroanalysis*, 16 (2004) 505
45. E.I. Iwuoha, S.E. Mavundla, V.S. Somerset, L.F. Petrik, M.J. Klink, M. Sekota and P. Baker, *Microchim. Acta*, 155 (2006) 453
46. K.M. Shaju, G.V.S. Rao and B.V.R. Chowdari, *J. Electrochem. Soc.*, 150 (2003) A1
47. Y. Feng, *Mater. Chem. Phys.*, 121 (2010) 302
48. B. Zhang, G. Chen, Y. Liang and P. Xu, *Solid State Ionics*, 180 (2009) 398
49. D. Linden and T.B. Reddy, eds. *Handbook of Batteries*. McGraw-Hill (2002)
50. A.J. Bard and L.R. Faulkner, *Electrochemical Methods_Fundamentals and Applications*, John Wiley & Sons, Inc (2001)
51. S.-M. Park and J.-S. Yoo, *Anal. Chem.*, 75 (2003) 455A
52. R. Greef, R.Peat, L.M. Peter, D. Pletcher and J. Robinson, *Instrumental methods in Electrochemistry - Southampton Electrochemistry Group*, Ellis Horwood (1990)
53. J. Chen, L. Yan and B. Yue, *J. Power Sources*, 209 (2012) 7
54. F. Gao and Z. Tang, *Electrochim. Acta*, 53 (2008) 5071
55. H. Liu, C. Li, H.P. Zhang, L.J. Fu, Y.P. Wu and H.Q. Wu, *J. Power Sources*, 159 (2006) 717
56. K. Tang, X. Yu, J. Sun, H. Li and X. Huang, *Electrochim. Acta*, 56 (2011) 4869